Astron. Astrophys. 333, 970–976 (1998)

ASTRONOMY AND ASTROPHYSICS

Radio flares from the active binary system UX Arietis

G. Torricelli-Ciamponi[1], E. Franciosini[2], M. Massi[3,4], and J. Neidhöfer[4]

[1] Osservatorio Astrofisico di Arcetri, Largo E. Fermi 5, I-50125 Firenze, Italy
[2] Dipartimento di Astronomia e Scienza dello Spazio, Largo E. Fermi 5, I-50125 Firenze, Italy
[3] Joint Institute for VLBI in Europe, Postbus 2, 7990 AA, Dwingeloo, The Netherlands
[4] Max-Planck-Institute für Radioastronomie, Auf dem Hügel 69, D-53121 Bonn, Germany

Received 8 December 1996 / Accepted 22 December 1997

Abstract. In this paper the flaring activity of the active binary system UX Arietis is investigated by analysing some radio spectra acquired by the Effelsberg 100-m radiotelescope. These spectra are characterized by positive spectral indexes, and show the evolution of the emission during the flare rising phases. The usual interpretation in terms of gyrosynchrotron emission from relativistic electrons trapped in a bipolar magnetic field and undergoing collisional and radiative losses does not fit these data. For this reason a continuous injection of accelerated particles has been included in the model. The computed spectra evolve in time in agreement with available observations.

Key words: binaries: close – stars: flare – stars: individual: UX Ari – radio continuum: stars

1. Introduction

UX Arietis belongs to the group of RS CVn stars, that are active binary systems characterized by the occurrence of strong flares in the X, UV and radio wavelengths domain. The system of UX Arietis has an orbital period of 6.44 days and is formed by a G5 V and a K0 IV star. The K star is the more active one and the presence of long-lasting large spots on its surface has been deduced from optical observations (Vogt & Hatzes 1991; Elias et al. 1995).

Radio emission from UX Arietis has been analysed by many authors (see Massi & Chiuderi Drago (1992) and references therein). To get a deeper insight on its flaring activity a monitoring program of this source was started in December 1992 at the Effelsberg 100-m telescope. The instrument was available for this program in the gaps between previously scheduled observations: for this reason our observations span a frequency interval between 1.4 GHz (21 cm) and 43 GHz (7 mm), depending on the scheduled receiver at each observing time. Most of these observations are made at a single frequency, but in a few cases it was possible to obtain some spectra. In this paper we will study the evolution of the flaring spectra, while the full data set will be described and analysed, searching for periodicities in the radio emission, in another paper (Massi et al. 1998). A preliminary presentation of the whole data set has been done by Massi et al. (1996), while results relative to the first six months of observations have been reported by Neidhöfer et al. (1993).

As described in Massi et al. (1996), a minimum is present in the observed flux densities around phase 0.4. This minimum can be easily interpreted in terms of a geometrical shadowing effect strictly linked to the rotation of the system. Since only the stronger emission suffers from the shadowing, while no effect is seen at lower flux levels, it follows that the high intensity emission is more localized (and organized, if one thinks in terms of magnetic field) than the low intensity one. This implies that the source is composed by a compact region, close to the star's surface, where the most intense emission mainly takes place, and by an extended halo, too large to be obscured, where the emission survives for a longer time and smoothly fades. This picture is in agreement with the conclusions derived from VLBI observations by Mutel et al. (1985) and with the model proposed by Franciosini & Chiuderi Drago (1995). Since the shadowing in the emission does not last very long (a small fraction of the orbital period) the compact region must have a typical size smaller than the stellar disk.

The presence of a geometric shadowing of the emission prevents the possibility of studying the evolution of a single flare on time scales longer than a few days. The modulation induced by the stellar rotation affects in fact the observed emission, reducing the flux density when the source is obscured. This implies that it is very difficult to have the opportunity of following the true evolution of the flaring emission from the flare onset to the end of the decaying phase. For this reason and for the way our data have been sampled, either the decaying or the rising phases of different flares are present in our data.

The decaying phase of flares has already been interpreted by Chiuderi Drago & Franciosini (1993) and by Franciosini & Chiuderi Drago (1995) as due to the temporal evolution of a population of non-thermal electrons, trapped in a magnetic loop and undergoing synchrotron and collision energy losses. In their model the injection of relativistic particles was assumed to be instantaneous, therefore the rising phase of the emission was not considered.

This paper is devoted to the analysis of the flare rising phase. For this purpose we have included in the above model a continu-

Send offprint requests to: G. Torricelli

ous injection of relativistic electrons, which makes the emission increase in spite of losses. The paper is organized as follows. The observed flare spectra are presented in Sect. 2; in Sect. 3 the time-dependent energy distribution of relativistic electrons is derived and in Sect. 4 the model results are compared with the observations. Conclusions are presented in Sect. 5.

2. Observed spectra during the rising phase

In spite of the difficulties outlined in the introduction, we can extract from the data some interesting examples of flaring activity. Among the available spectra of flares, we have selected those showing an increase in the measured flux density in a time interval of less than a few hours, which can be attributed to the rising phase. The data are plotted in Fig. 1, where different symbols refer to different orbital phases.

The following considerations are suggested by these figures. First of all, since the emission can increase only if an energy supply (in form of accelerated particles) is present, the time scale of the rise in the flux density gives an idea of the duration of the acceleration mechanism. From our observations we can infer that the particle acceleration can last, in some cases, for as long as two days (a phase difference of 0.01 corresponds to 1.54 hours); however, our data are sampled at long time intervals, and we cannot exclude that particles are accelerated in a succession of short time scale pulses, thus producing a series of bursts of shorter duration. Since we do not have the possibility to know the real substructure of the observed bursts, we will consider them as single flares. An example of "long-lasting energy injection" is shown in Fig. 1c (flare 3) where, at $\nu = 10.55$ GHz, the emission increases for as long as 23 hours.

The second important point is that, during active phases, the radiation received from UX Arietis has a positive spectral index ($\alpha > 0$ with $F_\nu \propto \nu^\alpha$) for 1.4 GHz $\leq \nu \leq$ 10 GHz, except for flare 4 where $\alpha > 0$ only for 1.4 GHz $\leq \nu \leq$ 5 GHz. The measured values of α are different from flare to flare and vary with time during the same flare, ranging from 0.31 to 0.73 between 2.7 and 5 GHz, and from 0.13 to 0.38 between 5 and 10.5 GHz, with the exception of flare 4, for which the latter is -0.11. These values agree with the spectral indexes measured in other RS CVn spectra, that, between 1.4 and 5 GHz, are in the range $-0.7 \leq \alpha \leq 1$ (Mutel et al. 1987), with higher values corresponding to higher luminosity periods. However, the spectra presented here show only positive spectral indexes in this frequency range, implying that this is a peculiarity of the flare rising phases. In fact, the peak present in the spectra at higher frequencies shifts in time towards lower frequencies and the spectral slope changes sign only when the emission is decreasing.

The common interpretation for positive spectral indexes at radio wavelengths is that of self-absorbed (gyro)synchrotron radiation. Dulk (1985) has derived approximate expressions for gyrosynchrotron emission from an homogeneous source in the case of an isotropic power-law electron energy distribution:

$$n(\gamma) = K(\gamma - 1)^{-\delta} \; ; \qquad (1)$$

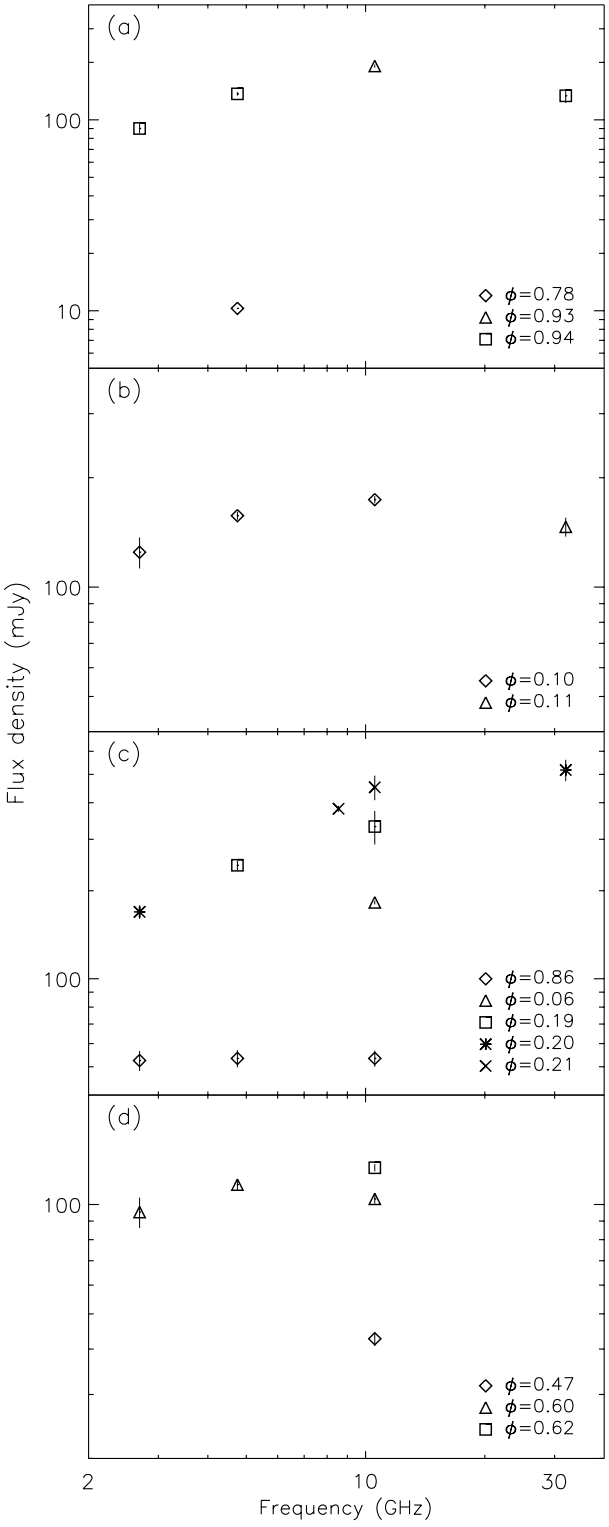

Fig. 1a–d. Observed flux density versus frequency at different times for four flares during the rising phase. **a** Flare 1: $\phi = 0.78$ corresponds to Julian Date 2448965.170; **b** Flare 2: $\phi = 0.10$ corresponds to J.D. 2449462.930; **c** Flare 3: $\phi = 0.86$ corresponds to J.D. 2449467.790; **d** Flare 4: $\phi = 0.47$ corresponds to J.D. 2449478.160

in this case the radiation spectrum at radio wavelengths has a positive self-absorbed spectral index

$$\alpha_{\rm self} = 2.5 + 0.085\delta \ , \qquad (2)$$

peaks at $\nu = \nu_{\rm peak}$ and decreases for $\nu > \nu_{\rm peak}$. However, the values of α measured for UX Arietis strongly deviate from the canonical slope (Eq. (2)). On the other hand, the observed spectrum cannot be interpreted as a consequence of the evolution of the distribution due to energy losses (collisional, radiative or other), since this kind of mechanism only affects the optically thin part of the spectrum (Chiuderi Drago & Franciosini 1993; Franciosini & Chiuderi Drago 1995). In addition, the data show that α deviates from the value 2.5 even when the flux density is increasing; indeed, during the rising phase the features of the spectrum cannot be ascribed to energy loss mechanisms only.

If we assume that gyrosynchrotron emission is the real emission mechanism, as widely accepted, the only possibility to explain the observed spectra is that geometrical effects influence the emitted radiation through the spatial distribution of the magnetic field. In fact, we can imagine the emission from a non-homogeneous source as the superposition of the contribution from many different homogeneous sources. Since the emission from each homogeneous part peaks at $\nu_{\rm peak}$, whose value depends mainly on the magnetic field strenght ($\nu_{\rm peak} \propto B^{0.68-0.06\delta}$, see Dulk 1985), the greater is the contribution from regions of high intensity field, the higher is the frequency at which the global spectrum peaks. In other words, the high frequency part of the spectrum comes from regions of strong magnetic field while the low frequency part is mainly due to the emission from regions of weak magnetic field. This implies that the diffuse and compact source components contribute to the emission at low and high frequencies, respectively. The superposition of different spectra can also explain why the optically thick ($\nu < \nu_{\rm peak}$) part of the observed spectrum has a slope different from $\alpha_{\rm self}$.

The above qualitative interpretation of the observed spectra suggests that a model intended to reproduce their evolution must include at least two features: a non-uniform source, which is necessary both for its influence on the spectral slope and for the observational evidence of a periodic shadowing of the emission (as outlined in the introduction); and a long lasting energy supply, needed to reproduce the increasing radio flux.

The time evolution of the electron population in a non-homogeneous magnetic field, when accelerated electrons are continuously injected in the source, is described in the following section.

3. The energy distribution of relativistic electrons

The energy distribution of the relativistic electrons responsible for the observed emission changes with time due to different types of losses, that depend on the environment where the emission takes place. Electrons are affected by synchrotron losses in the presence of the magnetic field, and undergo Coulomb collisions with the particles of the background thermal plasma.

A detailed study of the influence of the different types of loss mechanisms on the electron distribution have been developed for the analysis of the decaying phase of flares (see Franciosini & Chiuderi Drago 1995 and references therein). Generally speaking, Coulomb collisions have a typical time scale $t_{\rm coll} \simeq 10^9/N_{\rm e}$ hours, where $N_{\rm e}$ is the thermal electron density, while for synchrotron losses $t_{\rm syn} \simeq 10^4/B^2$ hours. In the case of UX Arietis the quoted values for the magnetic field range from ~ 10 G in the corona to 10^3 G at photospheric level, while an almost constant thermal density with $N_{\rm e} \sim 10^7 - 10^8$ cm^{-3} can be assumed (see Massi & Chiuderi Drago 1992 for details). Hence, collisional losses will influence the emission in the same way everywhere in the loop and on time scales of the order of ~ 1 day, while synchrotron losses will strongly suppress the emission from the compact region near the photosphere in a few minutes after the injection onset, but will affect the radiation from the extended coronal region only after some hours. Therefore, the consequences of radiative losses will be seen first at higher frequencies, while the low frequency emission coming from the diffuse region remains unaffected. The above considerations imply that radiative losses must be taken into account even during the rising phase of the flare, i.e., during the phase in which a large amount of new accelerated particles is injected in the loop.

In order to quantify how synchrotron and collision losses influence the electron distribution, it is necessary to define a specific model of the radio source. The geometry of the region where the flare energy is produced is not known, although the emission properties, related to the presence of the magnetic field, let us imagine loop-like structures analogous to those present in the solar corona. This picture is consistent with the one suggested in the previous section by the spectral shape and can also account for different radiative losses, as outlined above. In fact, in a magnetic loop anchored to the photosphere the compact region, whose emission peaks at higher frequencies, is the one which suffers from stronger radiative losses and the one which is more easily obscured by the stellar rotation. The extended coronal part of the loop emits longer and constitutes almost an halo around the star.

We assume here that the loop structure is the same of the model by Franciosini & Chiuderi Drago (1995), i.e. a dipolar magnetic field generated by a dipole buried under the stellar surface, and connecting two starspots of radius $R_{\rm spot}$ and angular separation Θ. The strength of the dipole is determined by the value $B_{\rm max}$ of the magnetic field in the center of the spots. As shown in Fig. 2, the magnetic field is described in terms of polar coordinates (r, Φ) on the plane perpendicular to the line of sight, where $\Phi = 90^\circ$ corresponds to the loop top and r is the distance from the dipole, and is assumed to be constant along the line of sight.

We suppose that electrons are injected at the top of the loop ($\Phi = 90^\circ$), uniformly, isotropically and at a constant rate. The dynamical time for relativistic electrons is very short, $t_{\rm dyn} \simeq R_*/c \simeq 7$ sec; hence, the injected electrons spread out rapidly from the acceleration site into the whole magnetic loop and, being reflected in the appropriate mirror points, reach in a

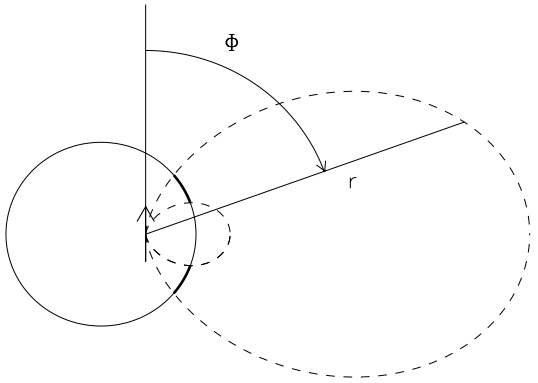

Fig. 2. A sketch of the magnetic field structure: the dashed curves identify the loop and the bold segments the starspots

very short time a definite spatial distribution. From our point of view, the attainment of this spatial distribution can be considered instantaneous since, for the moment, we have no way of investigating this short transient phase.

In order to derive the electron energy distribution as a function of space and time, we must solve the full kinetic equation. In our case, however, it is not possible to have any spatial resolution of the observed fluxes, so it has no sense to solve the equation exactly for the spatial dependence. Moreover, the time scales over which we are interested to investigate the effects of radiative and collision losses and of the continuous particle acceleration are much longer ($\sim hours$) than the dynamical time needed to attain a stationary distribution in absence of losses ($\sim seconds$). For this reason we decided to analyse the problem in two separate steps: we first derived the spatial density distribution just after the short transient phase neglecting energy losses. We then used this distribution as source function to study the time evolution including all losses (see Eq. (3)).

The solution of the kinetic equation along the magnetic field lines has been studied in the context of solar flares (see e.g. McTiernan & Petrosian 1990). For the first step we are interested in the stationary solution in the case of a non-uniform magnetic field and in the absence of losses. In the simplest case of an isotropically injected distribution at the loop top, as the one we are considering here, Leach & Petrosian (1981) show that the electron number density remains unaltered while electrons stream along the magnetic field lines and are reflected at the mirror points. This happens only if the thermal density scale height is larger than the magnetic one and if the adimensional column depth, $\tau \simeq 2\ 10^{-23} N_{\rm e} \Delta x$ (Δx is the coordinate along the loop axis), is smaller than one. This is the case for the emitting region in this binary system since an almost constant thermal density $N_{\rm e} \leq 10^8$ cm^{-3} is quoted (see before) and since the maximum loop length can not be larger than the binary separation $\Delta x \leq 3\ 10^{12}$ cm. Therefore, for times longer than the dynamical time the electron density is independent of the spatial coordinate. Thus, we can assume that relativistic electrons are injected uniformly and isotropically in the whole loop at a constant rate $Q(\gamma)$ el. cm^{-3} sec^{-1} and we can study how this uniform distribution evolves in time due to losses.

The equation describing the time evolution of the electron energy distribution, $n(\gamma,t)\,{\rm el./cm^3}$, in the case of injection plus energy losses is:

$$\frac{\partial n(\gamma,t)}{\partial t} + \frac{\partial}{\partial \gamma}\left[\frac{{\rm d}\gamma}{{\rm d}t}\, n(\gamma,t)\right] = Q(\gamma) - \nu_{\rm L}\, n(\gamma,t)\ , \qquad (3)$$

where

$$\frac{{\rm d}\gamma}{{\rm d}t} = -1.3\ 10^{-9} B^2\gamma^2 - 6.\ 10^{-13} N_{\rm e}\ {\rm sec}^{-1}\ , \qquad (4)$$

represents the energy variation due to synchrotron and collision losses, respectively, and $\nu_{\rm L}\, n(\gamma,t)$ represents the electrons that escape from the emitting region into the loss-cone. The loss-cone term has been evaluated by Franciosini & Chiuderi Drago (1995) as:

$$\nu_{\rm L} = \frac{\Omega_{\rm lc}}{2\pi\tau_{\rm d}} = \frac{(1-\cos\psi_\circ)}{\tau_{\rm d}}\ , \qquad (5)$$

where $\Omega_{\rm lc} = 2\pi(1-\cos\psi_\circ)$ is the loss-cone solid angle, with $\cos\psi_\circ = \sqrt{1 - B/B_{\rm max}}$, ($B$ = local magnetic field), and $\tau_{\rm d} \simeq 8.4\ 10^{11}\beta^3/N_{\rm e}$ sec ($\beta = v/c$) is the "deflection time" (Spitzer 1962), i.e. the characteristic time scale over which collisions with the background protons isotropize again the electron distribution.

The general solution of Eq. (3) is given by Melrose & Brown (1976) as

$$n(\gamma,t) = n(\gamma_\circ,0)\, {\rm e}^{H(\gamma)-H(\gamma_\circ)}\, \frac{\partial\gamma_\circ}{\partial\gamma} + \\ + \frac{1}{|{\rm d}\gamma/{\rm d}t|}\int_\gamma^{\gamma_\circ} Q(\gamma')\, {\rm e}^{H(\gamma)-H(\gamma')}\, {\rm d}\gamma'\ , \qquad (6)$$

where

$$H(\gamma) - H(\gamma') = \int_{\gamma'}^{\gamma} \frac{\nu_{\rm L}}{|{\rm d}\gamma''/{\rm d}t|}\, {\rm d}\gamma''\ , \qquad (7)$$

$\gamma_\circ$ is the electron energy at time $t = t_\circ = 0$ and the relation between γ and $\gamma_\circ$ can be derived by integrating Eq. (4) (see Chiuderi Drago & Franciosini 1993 for detailed calculations). The complete expression of the energy distribution at time t is obtained by carrying out the integral in Eq. (6) and substituting the relation $\gamma_\circ(\gamma,t)$. We have assumed for the injected energy distribution $Q(\gamma)$ and for the initial distribution $n(\gamma_\circ,0)$ the same functional dependence:

$$Q(\gamma) = Q_\circ K_\circ(\gamma-1)^{-\delta}\ , \qquad \gamma_{\circ 1} \leq \gamma \leq \gamma_{\circ 2} \qquad (8)$$

and

$$n(\gamma_\circ,0) = K_\circ(\gamma_\circ-1)^{-\delta}\ , \qquad \gamma_{\circ 1} \leq \gamma_\circ \leq \gamma_{\circ 2}\ . \qquad (9)$$

In the above expressions $K_\circ = n_\circ(\delta-1)(\gamma_{\circ 1}-1)^{\delta-1}$ and $n_\circ$ is the total electron number density at $t = 0$. The result of the integral in Eq. (6) depends on the value of γ: since at a given time t the distribution $n(\gamma,t)$ is defined for $\gamma \geq \gamma_1(\gamma_{\circ 1},t)$, while $Q(\gamma)$ is defined only for $\gamma \geq \gamma_{\circ 1} > \gamma_1$ (and is zero elsewhere), the effective integration limits are:

$$\gamma_{\rm min} = \begin{cases} \gamma & \gamma > \gamma_{\circ 1} \\ \gamma_{\circ 1} & \gamma \leq \gamma_{\circ 1} \end{cases} \qquad \gamma_{\rm max} = \begin{cases} \gamma_\circ & \gamma < \gamma_2 \\ \gamma_{\circ 2} & \gamma \geq \gamma_2 \end{cases}\ . \qquad (10)$$

4. Comparison with observations

Eqs. (6) and (7) derived in the previous section have been used to compute the gyrosynchrotron emission from a flaring loop. To calculate the plasma emissivity, j_ν, and the absorption coefficient, κ_ν, the results by Klein (1987) have been used. The only difference is that in our case the integration over the pitch angle has been performed numerically from $-\cos\psi_\circ$ to $+\cos\psi_\circ$, since the reflection at the mirror points makes the electron density n independent on ψ in the interval $-\cos\psi_\circ \leq \cos\psi \leq +\cos\psi_\circ$ and zero outside. In this calculation, the effect of the ambient plasma through free-free emission and absorption and the Razin effect have been also taken into account. The intensity is obtained integrating along the line of sight, s, as

$$I_\nu = \int j_\nu e^{-\kappa_\nu s} ds$$

where s is perpendicular to the loop projection as appears in Fig. 2. For simplicity every quantity has been assumed constant along s and the loop thickness is assumed proportional to r but independent on Φ (as in Franciosini & Chiuderi-Drago 1995). The successive integration of I_ν over the whole source, i.e. $\int_0^\pi d\Phi \int_{r_1(\Phi)}^{r_2(\Phi)} I_\nu(\Phi, r) r dr$ with r varying between the dipole lines of force ($r_1(\Phi)$ and $r_2(\Phi)$) shown in Fig. 2, yields the flux density. This last quantity can be compared with the observed radio spectra.

The resulting flux density is determined by the following parameters:

1) The spectral index δ of the initial and injected electron distributions. This parameter determines the slope in the optically thin region but is not crucial for the observed optically thick spectra; for this reason it has been arbitrarily fixed at reasonable values $\delta \sim 1.7 - 2$.

2) The thermal plasma density, N_e. Analyses of its effect on the emission by Massi & Chiuderi Drago (1992) and by Franciosini & Chiuderi Drago (1995) have determined an upper limit $N_\mathrm{e} \leq 10^7$ cm^{-3} for this quantity. We have assumed $N_\mathrm{e} = 10^7$ cm^{-3} for all the computed spectra.

3) The time $t_\circ$ at which the injection and hence the flare activity starts. It is not possible to infer $t_\circ$ from our data, since the flare onset can have occurred at any time between the observation of the first rising spectrum and a preceding observation of quiescent emission.

4) The magnetic field B_max at the base of the loop. As shown by Eq. (4), increasing the magnetic field makes radiative losses increase, and this results in a cutoff in the spectrum at lower and lower frequencies due to the suppression of the emission from higher energy electrons. The influence of the choice of B_max is clearly tied to the time interval $t - t_\circ$ during which synchrotron losses are important. The value of B_max has been chosen in order that, given $t - t_\circ$, it is possible to reproduce the observed position of the spectral peak.

5) The spot separation Θ, which determines the extension of the loop (in particular a big Θ makes the diffuse halo very large). In fact, a variation of Θ changes the relative importance of the regions at the footpoint and at the top, and hence it is determinant for changing the optically thick part of the spectrum. In particular, decreasing Θ gives a steeper spectrum at lower frequencies because it reduces the contribution from regions far from the star where the magnetic field is lower. The choice of Θ is however limited from the choice of R_spot to a range of values that give reasonable loop sizes.

6) The radius R_spot of the two starspots on the stellar surface on which the bipolar magnetic loop is anchored. Optical observations give typical spot radii $R_\mathrm{spot} \sim 18^\circ - 27^\circ$ (e.g. Elias et al. 1995); we have therefore considered values in this range.

7) The relativistic electron density $n_\circ$ at the flare onset ($t = t_\circ$). Its value defines a ground level of emission present before the start of the injection.

8) The injection rate $Q_\circ$ which, together with $n_\circ$, determines the intensity of the emission at any time after the start of the injection.

The method used to fit the observed spectra is the following. A ground level emission is reproduced assuming a given value for $t_\circ$ and deriving $n_\circ$. The evolution of the spectrum is then determined by choosing $Q_\circ$, B_max and Θ according to the observed characteristics of the following spectrum. The comparison of the theoretically predicted spectra at later times with the observed ones constitutes a test for the model.

The results are shown in Figs. 3–6 and the parameters used for the fits are given in Table 1. The values of Θ in Table 1 imply

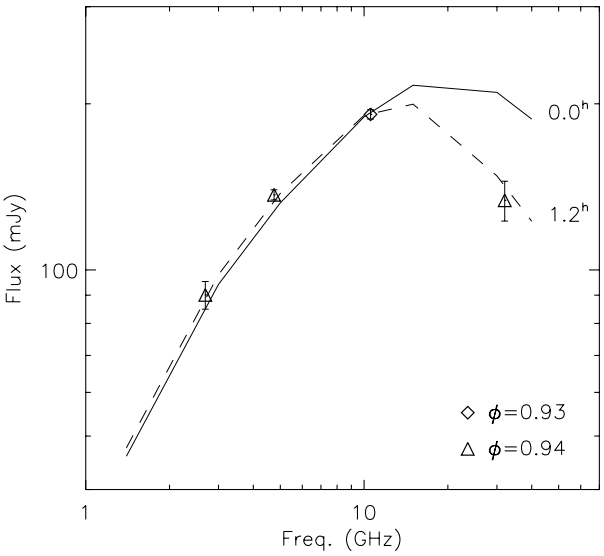

Fig. 3. Fit of flare 1 data at different times

Table 1. Parameters used for the fits of the observed flare spectra

	δ	Θ (°)	R_spot (°)	B_max (G)	$n_\circ$ (cm^{-3})	$Q_\circ$ (cm^{-3} s^{-1})
Flare 1	2.0	75	20	300	$1.23\,10^5$	$2.0\,10^{-5}$
Flare 2	1.7	90	20	1000	$2.2\,10^2$	$2.2\,10^{-3}$
Flare 3	2.0	50	20	500	$5.4\,10^5$	$4.4\,10^{-5}$
Flare 4	2.0	90	20	1000	$2.2\,10^3$	$1.7\,10^{-4}$

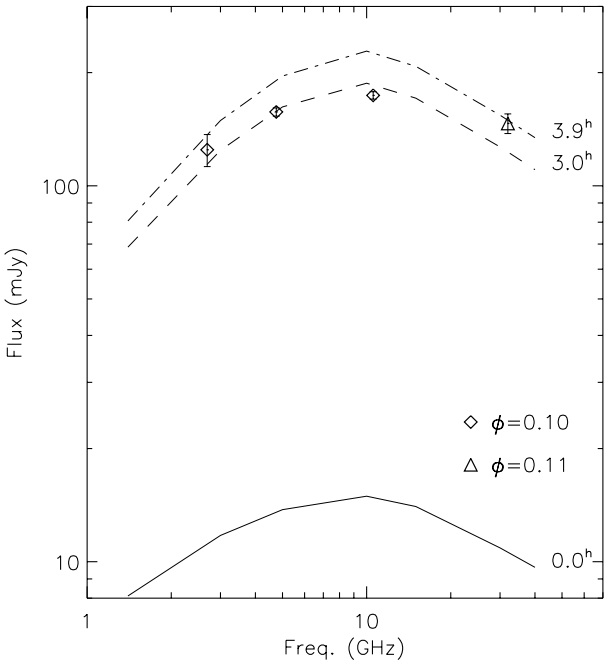

Fig. 4. Fit of flare 2 data at different times

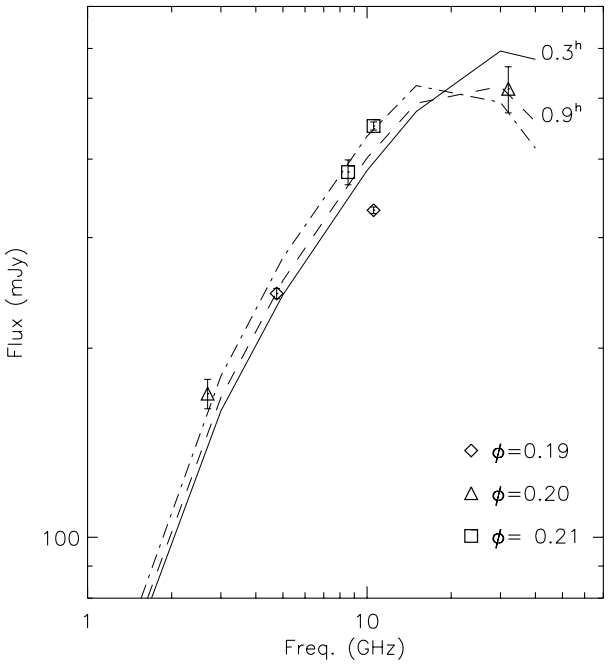

Fig. 5. Fit of flare 3 data at different times

very elongated loops, which in some cases extend to dimensions comparable to the binary system separation. The derived $B_{\max}$ is of the order or slightly lower than the photospheric values ($\sim 10^3$ G) derived from optical observations (Giampapa et al. 1983; Gondoin et al. 1985; Donati et al. 1990). These lower values are due to the fact that we do not "see" the emission originating near the photosphere (since it fades in a few seconds), but only the one coming from upper regions. In fact, the lower values are found in the case of flares 1 and 3, where we are observing a later phase, when the injection mechanism and hence the growth are almost over, as explained hereafter.

In Figs. 3–6 each spectrum is labeled with the time used in the calculation. This time has been derived from the exact time intervals between the observations, which is generally different from the one deduced from the approximated orbital phases shown in the figures. For flares 2 and 4 (Figs. 4 and 6, respectively) the ground level of emission at $t = t_\circ$ corresponds to the quiescent phase of the star. However, the assumption of a quiescent-like level of emission for the ground level, which seems the most obvious and elegant choice, is not always the best for our model. In fact, the evolution of the electron distribution has been derived for a *constant* injection rate and therefore the model must be applied in this limit. For example in the case of flare 1 the emission remains high but almost at the same level for a time $\Delta t \simeq 1$ hour, implying that the flare is near its maximum, i.e. in a phase where the electron injection is almost over. To reproduce such a case the only possibility is to assume a very low $Q_\circ$ in this time interval, but the same low value of $Q_\circ$ cannot reproduce the whole rising phase, starting from a quiescent flux of about 10 mJy. For this reason we have assumed $\phi = 0.93$ as starting time and the corresponding emission as ground level. The same happens for flare 3 where we have assumed that phase

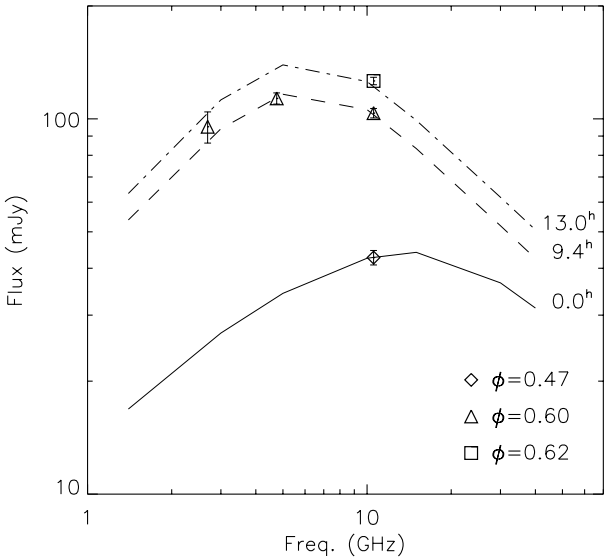

Fig. 6. Fit of flare 4 data at different times

$\phi = 0.19$ corresponds to $t - t_\circ = 0.3$ hours. Flares 2 and 4, for which the evolution can be followed from the beginning, clearly show the longest time evolution. In particular, in this framework it becomes clear that flare 4 is the only one to have a non-positive spectral index between 5 and 10 GHz because many hours have passed since the start of its rising phase.

It is apparent that the model reproduces remarkably well the time evolution of the spectra for the four flares considered in this paper. The physical implications are further discussed in the next section.

5. Conclusions

In this paper we have developed a model for the rising phase of some radio flares observed on the active binary system UX Arietis. Positive spectral indexes, lower than the canonical self-absorbed value (Eq. (2)), characterize the observed spectra for $\nu < 5$ GHz. These spectra can be explained in terms of gyrosynchrotron emission from a dipolar magnetic loop, where the lower regions, near the photosphere, contribute to the emission around 10 GHz, while the low-frequency part of the spectrum comes from the extended regions, upper in the corona, near the loop top. In this way the periodical minimum observed in the high frequency emission is easily explained as the shadowing of the compact part of the loop by the rotation of the system.

In addition to the loop-like geometry, in order to reproduce the observed spectral shape, both a continuous supply of relativistic electrons and loss mechanisms (synchrotron and collision energy losses and the effect of the loss-cone) must be taken into account. Among the eight parameters which must be defined to compute the emission three have been fixed in the correct range and have not been changed to improve the fit; two of them, namely $t_\circ$ and $n_\circ$ are determined by the less intense spectrum available for each flare; the three left parameters ($Q_\circ$, B_{max} and Θ) are chosen to fit the spectrum at the following time. This means that for each flare two spectra determine all the parameters of the model and that any subsequent time evolution of the flare spectrum is forecasted. Hence, for all the flares for which three spectra are available, the third one, i.e. the last one, is a prediction of the model.

The good agreement of the model results with the observed data confirms the interpretation of the flaring emission in terms of gyrosynchrotron emission from relativistic electrons continuously injected in a bipolar magnetic loop. How long this continuous supply of accelerated electrons lasts cannot be determined exactly. In the case of flare 3, for example, the data show that the emission increases for $\sim$ 23 hours; however our model, in which the number of injected electrons is constant in time, can reproduce only part of this evolution, namely 2 hours. This fact implies that the injection rate is not constant, but varies in time, and that the observed 23 hours growth is probably due to a succession of unresolved strong bursts, instead of a single event. In the case of flares 2 and 4, for which it is possible to follow the evolution starting from the "quiescent" ground level of emission, our model derives 4 and 13 hours respectively of constant injection. In any case, it is possible to conclude that the observed flare rising phases imply a continuous supply of relativistic electrons at least for some hours. The observations are however too sparse in time to allow a definite real comprehension of the process.

As Figs. 3–6 show, the model is able to reproduce flares having different spectral shapes and observed at different phases of their evolution. This large applicability of the model is assured by the complex interplay of radiative losses and continuous injection of fresh relativistic electrons. The very different values deduced for $Q_\circ$ and reported in Table 1 confirm the flexibility of the model. Flares observed near the peak of the rising phase (flares 1 and 3) have an almost vanishing injection rate while those observed in an earlier phase need higher values of $Q_\circ$ to be reproduced. Despite the interest and the originality of the data and the good results of the model reported in this paper, a deeper insight in the injection mechanism and hence in the physics of flares will be possible only with a model where the injection rate of accelerated electrons varies in time and is allowed to end at a certain time. However a more detailed model can give useful informations only if more complete data sets become available, with a better time coverage of the evolution of the flaring spectrum from its onset to the end of its decay.

Acknowledgements. We would like to thank the referee of the paper for his constructive criticism and his cooperation and Franca Chiuderi Drago for her fruitful comments. Maria Massi acknowledges support for her research by the European Union under contract FMGECT950012.

References

Chiuderi Drago F., Franciosini E. 1993, ApJ 410, 301
Donati J.-F., Semel M., Rees D.E., Taylor K., Robinson R.D. 1990, A&A 232, L1
Dulk G.A. 1985, ARA&A 23, 169
Elias II N.M., Quirrenbach A., Witzel A., et al., 1995, ApJ 439, 983
Franciosini E., Chiuderi Drago F. 1995, A&A 297, 535
Giampapa M.S., Golub L., Worden S.P. 1983, ApJ 268, L121
Gondoin P., Giampapa M.S., Bookbinder J.A. 1985, ApJ 297, 710
Klein K.-L. 1987, A&A 183, 341
Leach J., Petrosian V. 1981, ApJ 251, 781
Massi M., Chiuderi Drago F. 1992, A&A 253, 403
Massi M., Neidhöfer J., Torricelli Ciamponi G., Chiuderi Drago F. 1996, in: Radio Emission from the Stars and the Sun, ASP Conf. Ser. 93, Taylor A.R. & Paredes J.M. (eds.). ASP, S. Francisco, p. 330
Massi M., Neidhöfer J., Torricelli Ciamponi G., Chiuderi Drago F. 1998, A&A, in press
McTiernan J.M., Petrosian V. 1990, ApJ 359, 524
Melrose D.B., Brown, F.C. 1976, MNRAS 176, 15
Mutel R.L., Lestrade J.-F., Preston R.A., Phillips R.B. 1985, ApJ 289, 262
Mutel R.L., Morris D.H., Doiron D.J., Lestrade J.F. 1987, AJ 93, 1220
Neidhöfer J., Massi M., Chiuderi Drago F. 1993, A&A 278, L51
Spitzer L. 1962, Physics of fully ionized gases, Wiley, New York, p. 131
Vogt S.S., Hatzes A.P. 1991, in: The Sun and Cool Stars: Activity, Magnetism, Dynamos, IAU Coll 130, Tuominen I. et al. (eds). Springer, Berlin, p. 297